Desalination and Water Treatment
www.deswater.com

doi: 10.5004/dwt.2023.29532

293 (2023) 160–169
May

Citric acid-pyrolysis synthesis of bismuth titanate series compounds and their photocatalytic degradation

Yu ying Mo[a], Biyang Tuo[a,b,*], Jianli Wang[c], Guanghua Nie[a,b], Yun Tang[a,b]

[a]*School of Mining, GuiZhou University, Guiyang 550025, China, Tel. +86-18177164464; email: myy_gzu@163.com*
[b]*National and Local Joint Laboratory of Engineering for Effective Utilization of Regional Mineral Resources form Karst Areas, Guiyang 550025, Tel. +86-15286080806; emails: bytuo@gzu.edu.cn (B.Y. Tuo), 307885481@qq.com (G.H. Nie), 642205669@qq.com (Y. Tang)*
[c]*College of Material and Advanced Manufacturing, Hunan University of Technology, Zhuzhou 412000, email: whwangjianli@163.com*

Received 31 October 2022; Accepted 2 April 2023

ABSTRACT

Bismuth titanate based photocatalytic materials with different Bi/Ti ratios were synthesized by citric acid-pyrolysis method and used for the treatment of dye wastewater containing tartar yellow (TA). X-ray diffraction, UV-Vis diffuse reflectance spectroscopy, scanning electron microscopy, Fourier-transform infrared spectroscopy, X-ray photoelectron spectroscopy were used to analyze the performance of bismuth titanate based photocatalytic materials before and after the treatment of wastewater. The results showed that $Bi_{12}TiO_{20}$ prepared at a Bi/Ti ratio of 12:1, a metal ion to citric acid substance ratio of 1:1 and a roasting temperature of 600°C had a high photocatalytic activity and was able to achieve a degradation rate of 96.18% for TA and conformed to the proposed first order kinetic equation. The vacancies and superoxide radicals are the main active substances in the photocatalytic degradation process. $Bi_{12}TiO_{20}$ (Bi/Ti = 12:1) has a loose and porous mesh structure with good crystallinity and a forbidden band width of 2.41 eV. $Bi_{12}TiO_{20}$ (Bi/Ti = 12:1) has excellent stability and is expected to provide theoretical basis and guidance for TA dye wastewater treatment industry.

Keywords: Citric acid-pyrolysis method; Bismuth titanate; Tartar yellow; Photocatalytic degradation

1. Introduction

Over the past 20 years, the dyestuff industry has grown rapidly in Asia, particularly in China, Korea and India. As of today, China is the world's leading producer and exporter of dyestuffs, with annual dyestuff production reaching 900,000 tons, accounting for over 70% of the total global production of dyestuffs [1]. As one of the chemical industries with serious environmental pollution, the dyestuff industry brings economic benefits but generates a large amount of wastewater. Dyestuffs can be divided into natural and synthetic dyes depending on their source. 70% of synthetic dyes are based on azo structures. Azo acid dyes usually contain sodium salts of sulphonic and phenolic groups and insoluble in water, with the azo group (–N=N–) being the typical molecular structure possessed by these dyes [2]. Untreated dye wastewater discharged directly into water bodies can reduce water translucency, interfere with photosynthesis, thereby reducing dissolved oxygen levels and endangering aquatic life, causing serious environmental pollution problems and posing a health hazard [3]. Therefore, there is an urgent need for cost effective and environmentally friendly treatment processes to solve this pollution problem.

Currently, effective methods for treating azo dye wastewater include adsorption [4–10], coagulation [11], photocatalytic degradation [12–14], and membrane filtration [15,16]. Among them, photocatalytic degradation technology is a kind of green and sustainable technology that

* Corresponding author.

causes oxidation or reduction reaction by light-induced carrier excitation, and the organic reaction is realized under photocatalytic reactor, which has attracted much attention because of its high efficiency, no pollution and low-cost [17–19]. And the semiconductor photocatalyst represented by TiO_2 is a hot research topic in photocatalytic degradation technology for wastewater treatment. However, it greatly affects the photocatalytic activity due to its wide band gap and high hole-electron complexation rate [20], which usually needs to be modified. Bismuth-based catalysts have attracted the interest of researchers with their unique electronic structure and excellent visible light absorption ability. Among the new bismuth-based photocatalysts, BiOX (X = Cl, Br, I), Bi_2WO_6, $BiVO_4$, $Bi_4Ti_3O_{12}$, $Bi_{12}TiO_{20}$, $Bi_{20}TiO_{32}$, $Bi_2Ti_2O_7$, $Bi_2Ti_4O_{11}$ are regarded as promising photocatalysts, $Bi_4Ti_3O_{12}$, $Bi_{12}TiO_{20}$, $Bi_{20}TiO_{32}$, $Bi_2Ti_2O_7$ are commonly known as bismuth titanate compounds [21], bismuth titanate compounds are composite oxides formed by the compound of Bi_2O_3 and TiO_2, which have a small forbidden band width and excellent photocatalytic ability under visible light, giving them good potential for use in catalytic degradation. This study takes as its starting point the photocatalytic degradation of dye wastewater. In previous studies, bismuth titanate has often been used in photocatalyst studies, but few bismuth titanate series compounds have been prepared by altering Bi/Ti. In this paper, bismuth titanate series compounds were prepared by altering Bi/Ti using citric acid-pyrolysis and this was investigated around this point. In addition, reading through the extensive literature reveals that there are many different types of dye wastewater, but almost no studies on tartar yellow (TA), which are very widely used and which are a non-negligible hazard to the environment and humans, and are therefore used as the target pollutant in this study to investigate the optimum preparation conditions for bismuth titanate, and its photocatalytic degradation performance and mechanism.

2. Experiments

2.1. Synthesis of bismuth titanate

Bismuth nitrate pentahydrate, tetrabutyl titanate, citric acid and tartaric yellow were purchased from China National Pharmaceutical Chemical Reagent Co. All chemicals were of analytical grade and the water used for the experiments was distilled water. According to the method proposed in the literature [22], the reactants bismuth nitrate pentahydrate ($Bi(NO_3)_3{\cdot}5H_2O$) and tetrabutyl titanate ($C_{16}H_{36}O_4Ti$), weighed in stoichiometric ratios of 20:1, 16:1, 12:1, 8:1, 4:1, 4:3 and 1:1, were added to a certain amount of citric acid ($C_6H_8O_7{\cdot}H_2O$), put together into an agate mortar and grind well, put into a muffle furnace at 500°C for 10 min, took out the reaction product and grind it well, then the precursor was ready. The precursor was then roasted at 600°C for 3 h. After natural cooling and grinding, the Bi/Ti materials were obtained as 20:1, 16:1, 12:1, 8:1, 4:1, 4:3 and 1:1 bismuth titanate materials, respectively. In addition, the synthesized materials with Bi/Ti of 12:1 were roasted at 450°C, 500°C, 550°C, 600°C, 650°C and 700°C for 3 h to investigate the phase states of the bismuth and titanium compounds.

To investigate the effect of citric acid dosage, four groups of citric acid were weighed and numbered. The first group of citric acid was 2.4978 g, the second group of citric acid was 2.9970 g, the third group of citric acid was 3.7463 g, and the fourth group of citric acid was 4.9951 g. The ratios of citric acid to the amount of metal ions present in the precursor were 1:1, 1.2:1, 1.5:1 and 2:1, respectively (note N1 as 1:1, N2 is 1.2:1, N3 is 1.5:1 and N4 is 2:1). The bismuth titanate (12:1) material was prepared under the same conditions.

2.2. Characterisation of materials

X-ray diffractometry (XRD) was used to analyse the crystalline structure, phase type of the prepared photocatalysts under Cu target Kα radiation, a scan rate of 2°/min^{-1}, a scan range of 5° to 90°, a voltage of 40 kV and a current of 40 mA (Bruker AXS D8 Advance, Germany). Surface elements and micromorphology of the materials were obtained by scanning electron microscopy (SEM) and energy-dispersive X-ray spectroscopy (EDX) (ZEISS Gemini 300, Germany). UV-Vis diffuse reflectance spectroscopy was used to measure the light absorption properties of bismuth titanate in the range 200–800 nm (Shimadzu UV-3600i Plus, Japan). Fourier-transform infrared spectroscopy (FTIR) was used to analyze the chemical bonds and functional groups of the photocatalyst, the scanning number was 32 and the scanning wave number was 4,000–400 cm^{-1} (Thermo Scientific Nicolet iN10, USA). X-ray photoelectron spectroscopy (XPS) was used to analyze the element composition and chemical morphology of the surface of photocatalysis materials, the spectrum were calibrated to the C 1s peak at 284.8 eV (Thermo Scientific K-Alpha, USA).

2.3. Adsorption of materials

Bismuth titanate (0.1 g) was placed in TA solution (100 mL, 5 mg/L) and stirred in a dark oven for 30 min. 4 mL of the solution was taken every 5 min. After centrifugation, the absorbance of the TA solution was measured at 427 nm. The amount of TA adsorbed can be calculated using Eq. (1):

$$q_t = \frac{(C - C_t)V}{W} \tag{1}$$

where q_t is the adsorption capacity at time t, mg/g; C is the initial concentration of TA solution, mg/L; C_t is the concentration of TA at time t, mg/L; V is the initial volume of TA solution, L; W is the weight of bismuth titanate, g.

2.4. Photocatalytic performance testing

Bismuth titanate (0.1 g) was placed in TA solution (100 mL, 5 mg/L) and stirred magnetically in a dark box for 30 min to achieve adsorption–desorption equilibrium between the catalyst and the reaction solution; the reaction was then carried out under the irradiation of a xenon lamp (500 W) for 150 min, with 4 mL sampled every 30 min. The supernatant was then centrifuged and the absorbance of TA was measured using a UV-spectrophotometer. The absorbance at 427 nm was used to calculate the

concentration change of TA in the presence of the catalyst and to evaluate the catalytic ability of the photocatalyst.

The degradation rate of TA is calculated by Eq. (2):

$$\eta = \frac{C - C_t}{C} = \frac{A - A_t}{A} \quad (2)$$

where η is the TA degradation rate, %; C is the initial concentration of TA solution, mg/L; C_t is the concentration of TA solution after light exposure time t, mg/L; A is the initial absorbance of the TA solution; A_t is the absorbance of the TA solution after light exposure time t.

3. Results and discussion

3.1. Structure, composition and microscopic morphology of bismuth titanate composites

The XRD of four ratios of bismuth titanate composites (Bi/Ti = 20:1, 12:1, 1:1, 4:3) prepared at N1, roasting temperature of 600°C is shown in Fig. 1. The diffraction peaks at 24.7°, 27.7°, 30.4°, 32.9°, 52.3°, 55.6°, 61.7° at Bi/Ti = 20:1 and Bi/Ti = 12:1 correlate well with the cubic crystal system (JCPDS NO. 78-1158) corresponding to the (220), (310), (222), (222), (321), (035), (611), (631) and (631) crystal planes of $Bi_{12}TiO_{20}$, respectively. In addition, no $Bi_{20}TiO_{32}$ material was found in the manually measured peaks, indicating that this method can be used for the synthesis of $Bi_{12}TiO_{20}$; for Bi/Ti = 4:3, mainly $Bi_4Ti_3O_{12}$ and a small amount of $Bi_{12}TiO_{20}$ in the cubic crystal system, with the diffraction peak at 2θ = 32.9° attributed to the (321) crystal plane of $Bi_{12}TiO_{20}$ (JCPDS NO. 34-0097); When Bi/Ti = 1:1, the diffraction peak of the crystalline plane of the bismuth titanate material coincides with the standard card JCPDS NO. 32-0118, and the peak shape is sharp, indicating that the material is $Bi_2Ti_2O_7$. The above analysis results show that different bismuth titanates can be synthesized by adjusting the molar ratio of Bi to Ti when using the citric acid-pyrolysis method to prepare bismuth titanate materials. The citric acid-pyrolysis method can be used for the synthesis of $Bi_{12}TiO_{20}$, but not for $Bi_{20}TiO_{32}$.

In order to investigate the best conditions for the preparation of bismuth titanate compounds, $Bi_{12}TiO_{20}$ materials were prepared by varying the amount of citric acid and the roasting temperature. The XRD patterns is shown in Fig. 2a. The diffraction peaks of the material are in good agreement with the standard card JCPDS NO. 78-1158, and the $Bi_{12}TiO_{20}$ material is well crystallized, which indicates that the physical phase of the material is not affected by changing the amount of citric acid. The strongest intensity of the $Bi_{12}TiO_{20}$ diffraction peak at N1 indicates that Bi_2O_3 and TiO_2 can synthesize bismuth titanate to the greatest extent when Bi/Ti = 12:1, indicating that the addition of citric acid plays a key role in the preparation of bismuth titanate, and citric acid reacts with metal ions in a complex,

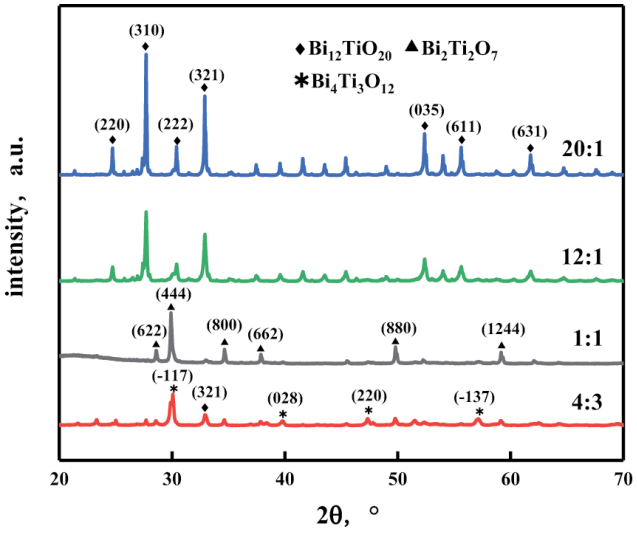

Fig. 1. X-ray diffraction patterns of four Bi/Ti preparations of bismuth titanate composites.

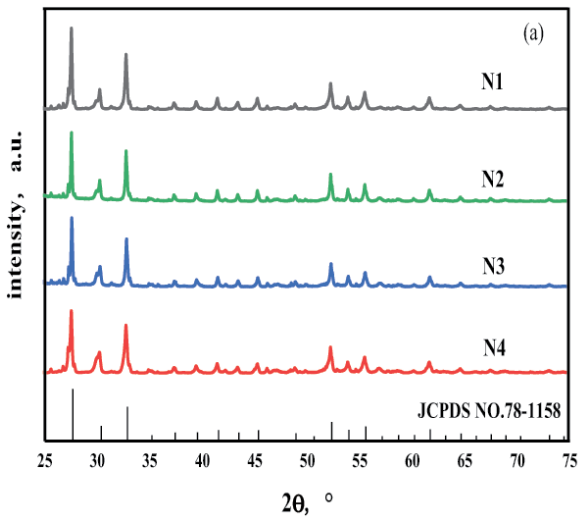

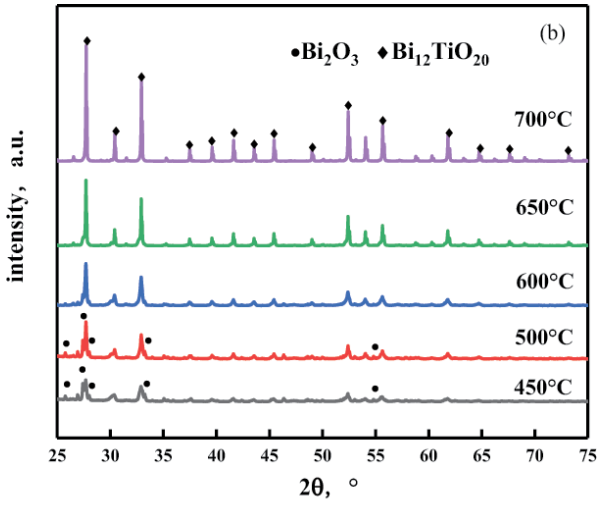

Fig. 2. (a) X-ray diffraction patterns of $Bi_{12}TiO_{20}$ prepared with different amounts of citric acid and (b) X-ray diffraction patterns of $Bi_{12}TiO_{20}$ prepared at different roasting temperatures.

and then forms stable bismuth titanium citrate complexes. Fig. 2b shows the XRD patterns of $Bi_{12}TiO_{20}$ prepared at different temperatures. When the temperature was lower than 600°C, the material appeared the heterogeneous phase Bi_2O_3, and did not completely form $Bi_{12}TiO_{20}$; when the temperature was greater than or equal to 600°C, the heterogeneous phase Bi_2O_3 disappeared and completely formed $Bi_{12}TiO_{20}$. Therefore, the higher the temperature, the better the degree of crystallization of bismuth titanate, which was beneficial to the formation of bismuth titanate.

The SEM microanalysis morphology and structure of four ratios of bismuth titanate (Bi/Ti = 20:1, 12:1, 1:1, 4:3) are shown in Fig. 3. The material in Fig. 3a (Bi/Ti = 20:1) has a ginger-like structure. The surfaces are all irregularly curved and loaded with small particles. In Fig. 3b, the prepared $Bi_2Ti_2O_7$ material particles are spherical or ellipsoidal in shape, with an unsmooth surface and severe agglomeration. When Bi/Ti = 4:3, the morphology of the material is polyhedral and lamellar with regular surface and serious agglomeration. Fig. 3d shows a reticulated porous structure of $Bi_{12}TiO_{20}$ material and arranged in flakes, with fibrous material and small particles attached to the surface of the material. The reticulated porous structure facilitates light harvesting, charge separation, utilisation of active sites and more exposed interface contact with reactants [23]. The $Bi_{12}TiO_{20}$ material prepared in Fig. 3 is well dispersed, while the remaining two materials show agglomeration. To further determine the chemical composition, this is illustrated by an EDX spectrum, in Fig. 3e, in addition to the spectral peaks belonging to the elements C and O, there are also spectral peaks of Ti and Bi, which can confirm the successful synthesis of bismuth titanate by this method.

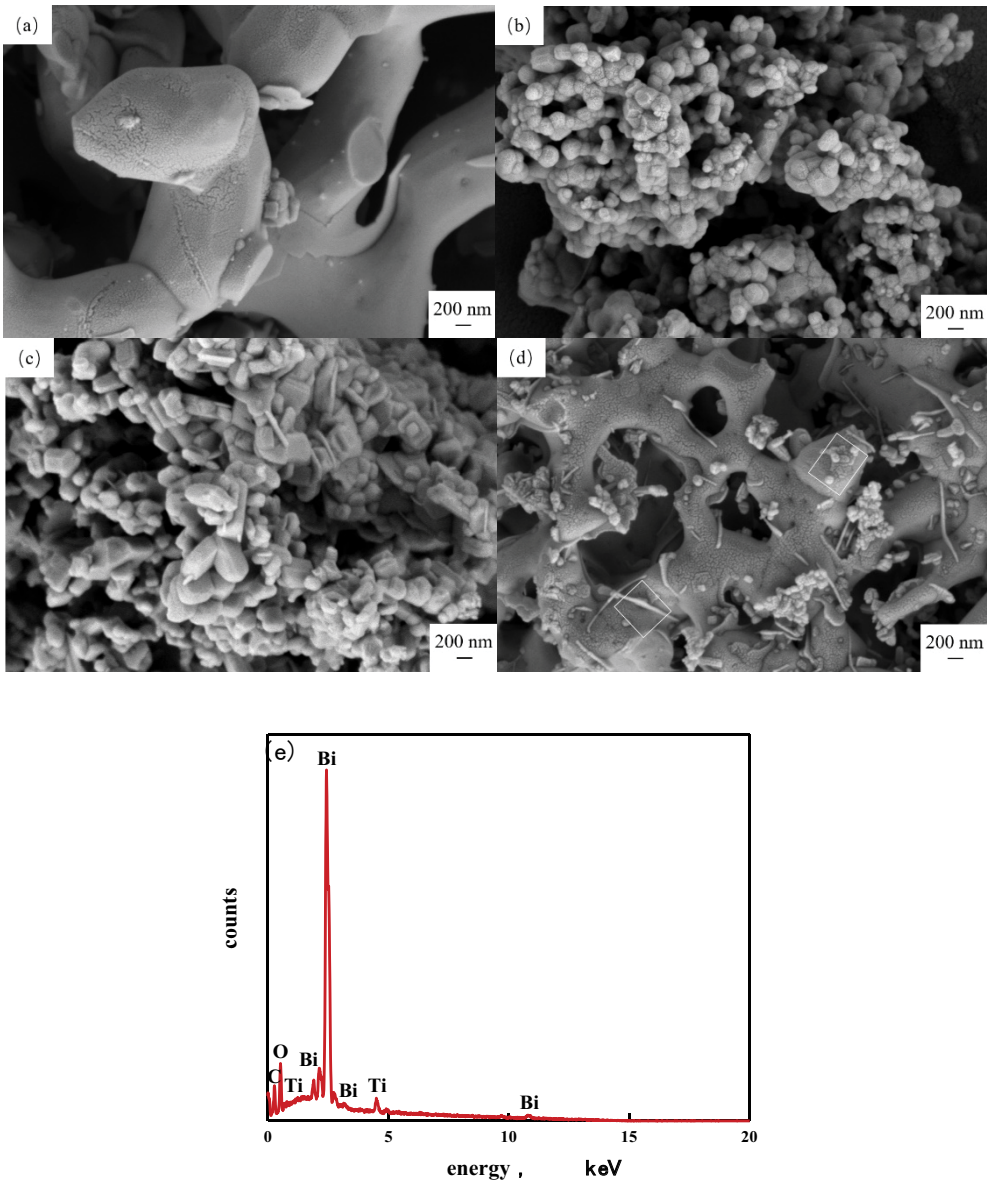

Fig. 3. Scanning electron microscopy images of Bi/Ti = 20:1 (a), Bi/Ti = 1:1 (b), Bi/Ti = 4:3 (c), Bi/Ti = 12:1 (d) and energy-dispersive X-ray spectrum of Bi/Ti = 12:1 (e).

The FTIR spectra of TA before and after adsorption are depicted in Fig. 4. $Bi_{12}TiO_{20}$ exhibits two dense peaks at 1,389.20 and 1,472.17 cm^{-1} that are assigned to the ν_3 vibrational mode of the TiO_4 tetrahedral unit of $Bi_{12}TiO_{20}$.

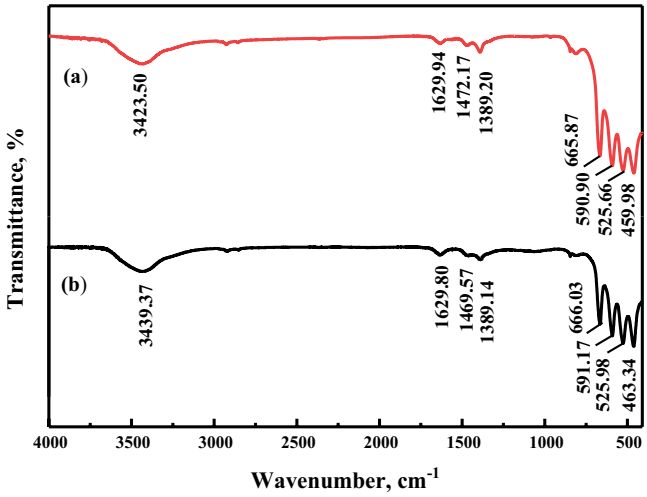

Fig. 4. Fourier-transform infrared spectrum of $Bi_{12}TiO_{20}$ (a) before and (b) after adsorption of tartar yellow.

Asymmetric stretching vibrations of Ti–O–Ti occur at 1,389.20 cm^{-1}. while the 459.98, 525.66, 590.90 and 665.87 cm^{-1} are all attributed to the Bi–O vibrational mode, corresponding to the characteristic peaks of silica ferrite [24]. The stretching and bending vibrations of water occur at 3,423.50 and 1,629.94 cm^{-1}, respectively, the former corresponding to the stretching vibration of the OH group attached to the titanium atom (Ti–OH) and the latter to the bending vibration of the OH in the water adsorbed in the sample [25]. The intensity of the vibrational bands of many groups changes or shifts slightly in position after the adsorption of TA by $Bi_{12}TiO_{20}$. The bands at 3,423.50, 665.87, 590.90 and 459.98 cm^{-1} were shifted to higher bands at 3,439.37, 666.03, 591.17 and 463.34 cm^{-1}, respectively, and conversely, the peak at 1,472.17 cm^{-1} was shifted to a lower band at 1,469.57 cm^{-1}. After the adsorption of $Bi_{12}TiO_{20}$ the shifts of the different active functional groups suggest that their epitope sites may interact with TA ions, but due to the small overall changes, physical adsorption played a dominant role in the adsorption process.

In order to study the composition and chemical state of the prepared bismuth titanate compounds, $Bi_{12}TiO_{20}$ was further analyzed by XPS measurement. The XPS measurement spectrum of $Bi_{12}TiO_{20}$ powder is shown in Fig. 5a. XPS peak showed that the catalyst contained only Bi, Ti and O

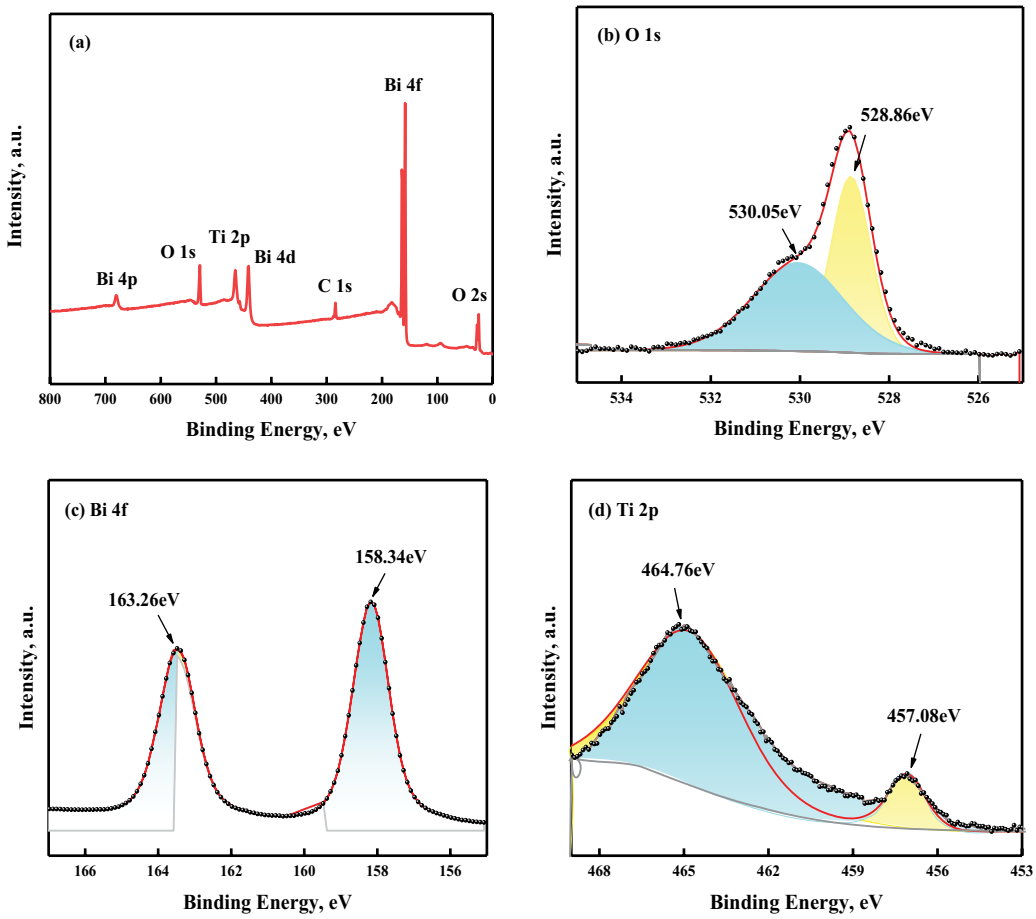

Fig. 5. (a) X-ray photoelectron spectra of $Bi_{12}TiO_{20}$, (b) O 1s XPS spectra of $Bi_{12}TiO_{20}$, (c) Bi 4f XPS spectra of $Bi_{12}TiO_{20}$ and (d) Ti 2p XPS spectra of $Bi_{12}TiO_{20}$.

elements and a trace amount of carbon. Fig. 5b–d illustrate the high-resolution XPS spectra of O 1s, Bi 4f and Ti 2p. With respect to the XPS spectra of O 1s in Fig. 5b, the peak at 530.05 eV should be attributed to the lattice oxygen O^{2-} of the Bi–O band in $Bi_{12}TiO_{20}$. The peak at 528.86 eV belongs to the surface hydrocarbon group [26]. The two binding energy peaks centered on 158.34 and 163.26 eV in Fig. 7b were assigned to Bi^{3+}. As shown in Fig. 5d, the position of double peak at 457.08 and 464.76 eV indicates that Ti exists in the form of Ti^{4+} in the composite. Consequently, the XPS results confirmed the successful preparation of $Bi_{12}TiO_{20}$.

3.2. Optical properties

The UV-Vis diffuse reflectance spectroscopy of the four materials are shown in Fig. 6. The main light absorption regions and light absorption edges of the four materials in Fig. 6a are in the visible range (390–780 nm). $Bi_{12}TiO_{20}$ material absorbs visible light more intensely than the other two for Bi/Ti = 20:1 and Bi/Ti = 12:1, and there is a significant red-shift phenomenon. The band gap of the composite can be calculated according to Eq. (3):

$$(\alpha h\nu)^{1/n} = A(h\nu - E_g) \quad (3)$$

where α is the light absorption index; h is the Planck constant; v is the optical frequency; A is a constant; E_g is the band gap energy. The n value is determined by the optical transition type of the semiconductor (for direct leaps, n = 1/2; for indirect leaps, n = 2) [26]. Here, the prepared material n value can be specified as 2.

In Fig. 6b the forbidden band widths of the four materials (Bi/Ti = 20:1, 12:1, 1:1, 4:3) calculated according to Eq. (3) are: 2.25, 2.41, 2.64, and 2.47 eV, all of which can absorb visible light. The content of Bi elements can adjust the rate of electron separation complex in photogenerated carriers [25], the higher the content of Bi elements, the smaller the band gap and the faster the rate of electron–hole separation complex in photogenerated carriers, which is more favourable to the absorption of visible light.

3.3. Adsorption

The molar ratio of Bi to Ti was continued at N1, roasting temperature of 600°C, and seven different ratios of the materials were prepared to investigate their adsorption properties. As shown in Fig. 7, when the Ti content is constant, the Bi content is greater than 12 or less than 12, and the adsorption capacity of the material is lower than 0.4 mg/g. When Bi content is 12, it shows the highest adsorption, which is mainly due to the loose porous network structure, which is conducive to the dispersion and adsorption of dye molecules. When Bi/Ti = 1:1, $Bi_2Ti_2O_7$ was formed, the adsorption capacity was enhanced, but the agglomeration was serious, which made the adsorption capacity not high. Bi/Ti = 4:3, $Bi_4Ti_3O_{12}$ and a small amount of $Bi_{12}TiO_{20}$ were formed, the irregular polyhedral and lamellar structure also made the adsorption capacity enhanced, but the agglomeration phenomenon inhibited the adsorption capacity. The adsorption rates for all seven materials were fastest in the first 5 min,

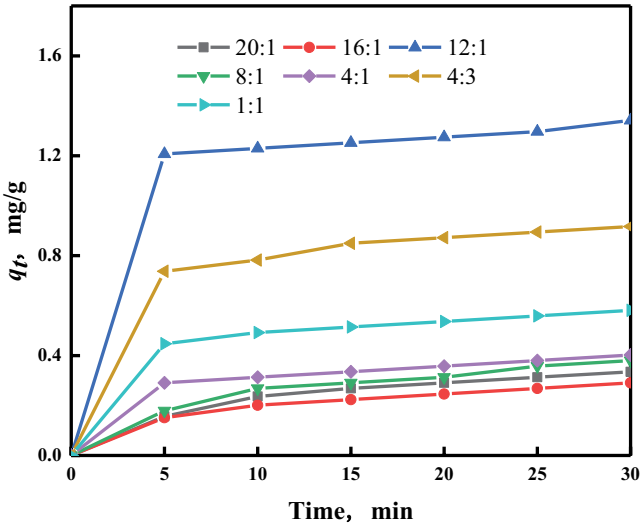

Fig. 7. Effect of different Bi/Ti materials on the adsorption of tartar yellow.

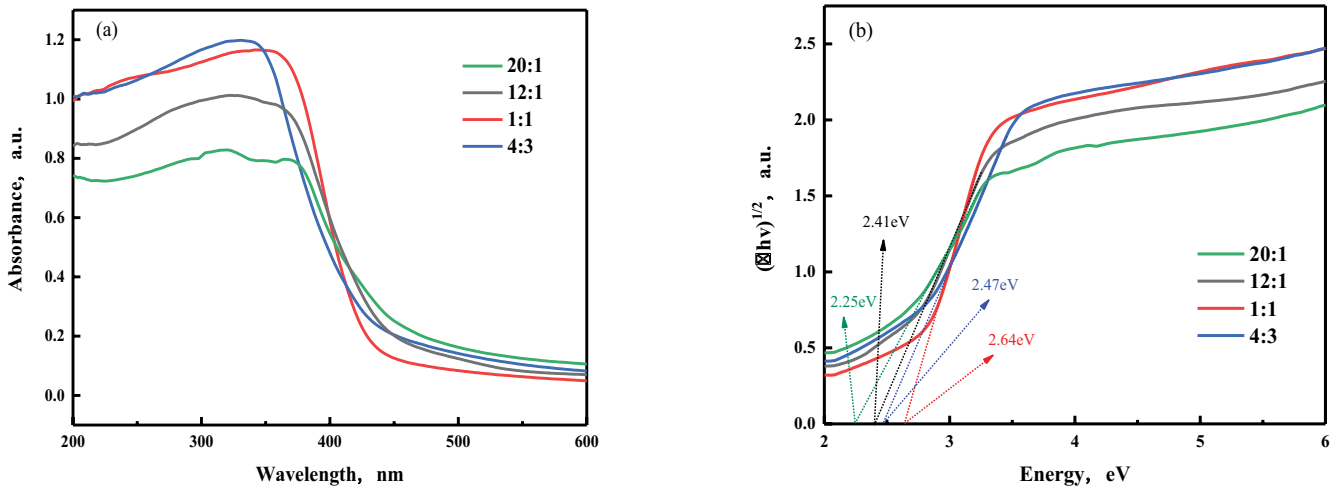

Fig. 6. UV-Vis diffuse reflectance spectroscopy spectra of four materials (Bi/Ti = 20:1, 12:1, 1:1, 4:3).

slowing down with increasing contact time and eventually reaching adsorption–desorption equilibrium. The faster adsorption in the first 5 min is due to more adsorption sites being available in the early stages and the difficulty in occupying the remaining sites due to repulsion between solute and phase in the later stages [27].

3.4. Photocatalytic performance

The effect of Bi/Ti on the degradation rate of TA was investigated by fixing N1, roasting at 600°C and adjusting Bi/Ti to 20:1, 16:1, 12:1, 8:1, 4:1, 4:3 and 1:1, respectively, and the results are shown in Fig. 8a. As can be seen from Fig. 8, the $Bi_{12}TiO_{20}$ material formed at Bi/Ti = 12:1 showed the highest degradation rate of TA after 150 min of light exposure, reaching 96.18%, and was much higher than the other six materials. Continuing to refine the molar ratio of Bi and Ti, fixing the Ti content and changing only the Bi content of the synthesized bismuth titanate, the photocatalytic effect of several other materials synthesized under Bi/Ti was not satisfactory, except for the bismuth titanate synthesized at Bi/Ti = 12:1, where the degradation rate was 56.12% at Bi/Ti = 16:1 and only 40% at Bi/Ti = 1:1. It indicates that the bismuth-titanium ratio is an important factor affecting the photocatalytic activity of bismuth titanate materials prepared by the citric acid-pyrolysis method, and the best photocatalytic performance of $Bi_{12}TiO_{20}$ synthesized by this method was achieved at Bi/Ti = 12:1. Analysis in the study of $Bi_{12}TiO_{20}$ single crystals revealed that the crystal structure of non-doped $Bi_{12}TiO_{20}$ generally exhibited a non-chemometric ratio, with vacancies of Ti atoms above 10% and the presence of intrinsic point defects due to vacancies in the Ti atoms. Some of the vacant Ti^{4+} in the TiO_4 tetrahedra are replaced by Bi^{3+}, while generating a positive hole on the adjacent oxygen atom in the tetrahedra [28], and this production of these holes also results in the strong absorption of $Bi_{12}TiO_{20}$ in the visible region. This is followed by the synthesis of $Bi_4Ti_3O_{12}$ and $Bi_{12}TiO_{20}$ coexisting bismuth titanate at Bi/Ti = 4:3, which degrades 64.41% of TA.

The pseudo-first-order kinetic was used to fit the kinetics of photocatalytic degradation of TA solutions by bismuth titanate synthesized with different Bi/Ti, which can be calculated using Eq. (4):

$$\ln\left(\frac{C_0}{C_t}\right) = kt \tag{4}$$

where C_0 is the TA solution after dark adsorption, mg/L; C_t is the concentration of TA solution after light exposure time t, mg/L; t is the time of light irradiation, min; k is the rate constant of the proposed primary reaction, min^{-1}.

Fig. 8b shows the results of the fit. The degradation of TA by bismuth titanate synthesized with different Bi/Ti fits the pseudo-first-order kinetic equations. The k-value of $Bi_{12}TiO_{20}$ synthesised at Bi/Ti = 12:1 was the largest at 0.01983 min^{-1}, with increasing or decreasing Bi content, the k-values of the synthesised bismuth titanate were smaller, proving that the photocatalytic effect on TA was not satisfactory. It was further demonstrated that Bi/Ti was suitable for the best photocatalytic effect on TA when bismuth titanate was prepared by the citric acid-pyrolysis method.

Bi/Ti was 12:1, the roasting temperature was 600°C and the citric acid addition was changed to N1, N2, N3 and N4 to investigate the effect of different citric acid dosages on the degradation rate of TA, the results are shown in Fig. 9a. In the preparation of $Bi_{12}TiO_{20}$, the metal ion to citric acid ratio of 1:1 resulted in the largest TA degradation rate of 96.18%, while N2, N3 and N4 could only remove 78.87%, 74.79% and 83.84%. Based on the XRD results, it shows that the N1 material has the best crystallinity. The effect of roasting temperature on the degradation of TA of the material was investigated by fixing N1, Bi/Ti was 12:1 and varying the roasting temperatures of 450°C, 500°C, 550°C, 600°C, 650°C and 700°C, respectively, and the results are shown in Fig. 9b. The $Bi_{12}TiO_{20}$ material prepared at the roasting temperature of 550°C already had good catalytic activity. When the roasting temperature was lowered, the photocatalytic activity decreased due to the incomplete formation of $Bi_{12}TiO_{20}$ in the first stage; the highest catalytic activity was obtained for the $Bi_{12}TiO_{20}$ material prepared at a roasting temperature of 600°C; when the roasting temperature

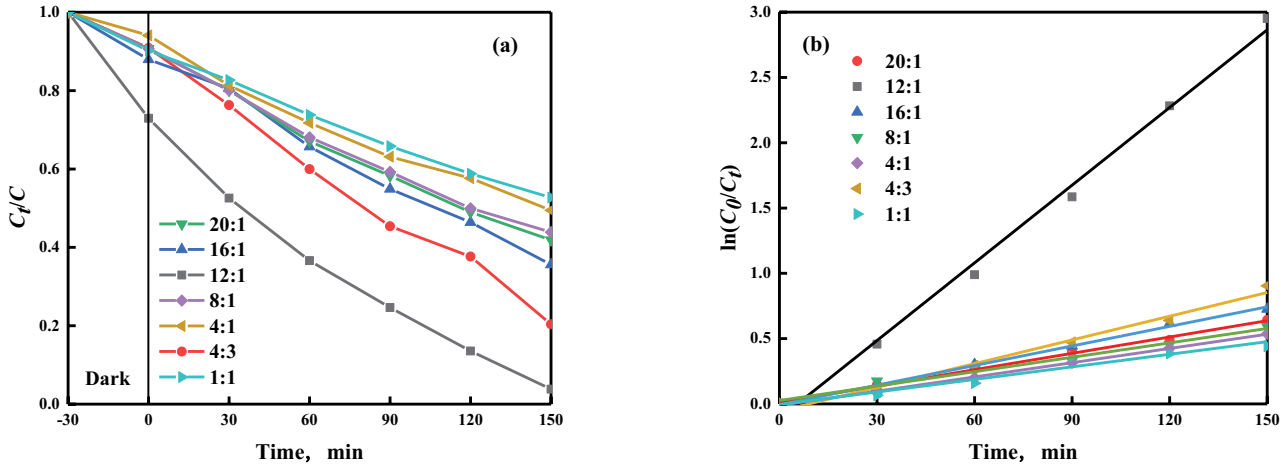

Fig. 8. Degradation curves of tartar yellow (a) photocatalytic degradation of tartar yellow by materials with different Bi/Ti and (b) pseudo-first-order kinetic for different catalysts.

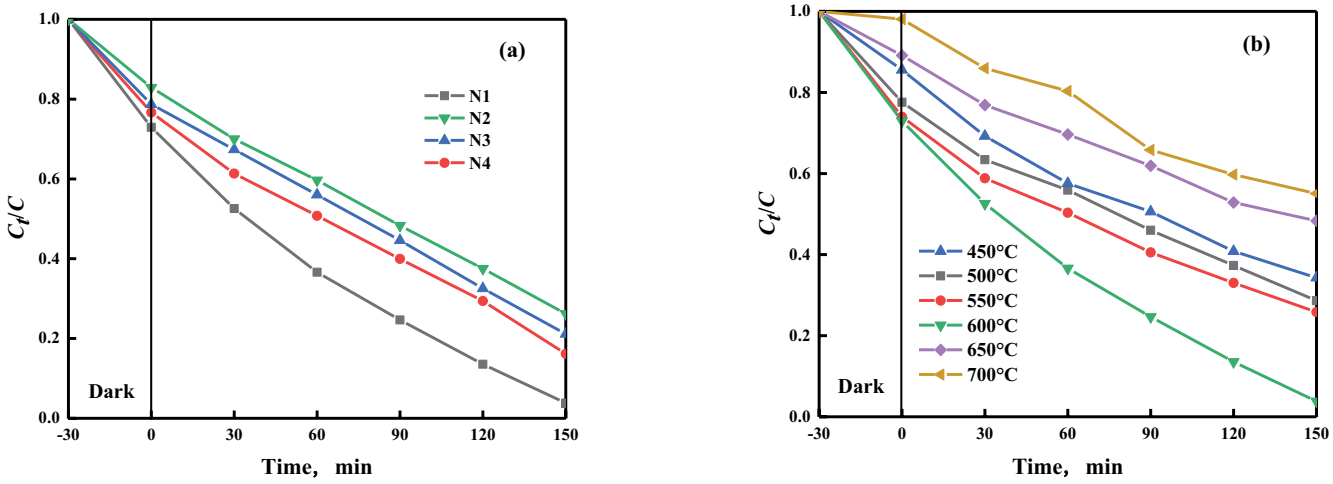

Fig. 9. Tartar yellow degradation curves (a) $Bi_{12}TiO_{20}$ prepared at different citric acid additions and (b) $Bi_{12}TiO_{20}$ prepared at different roasting temperatures.

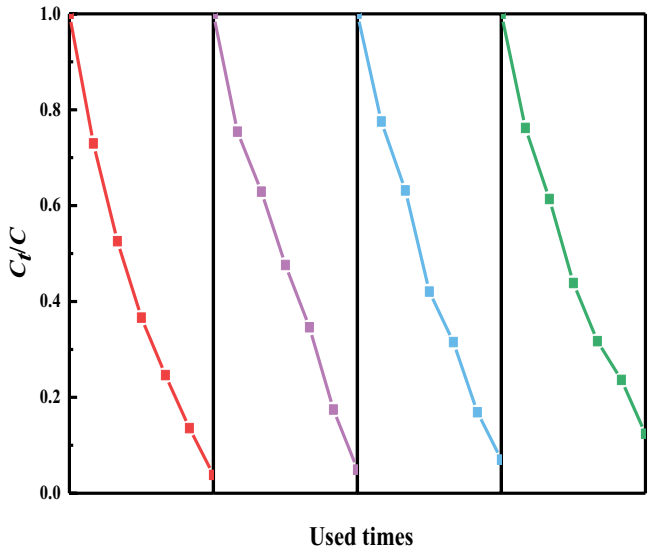

Fig. 10. Stability test of $Bi_{12}TiO_{20}$ (Bi/Ti = 12:1).

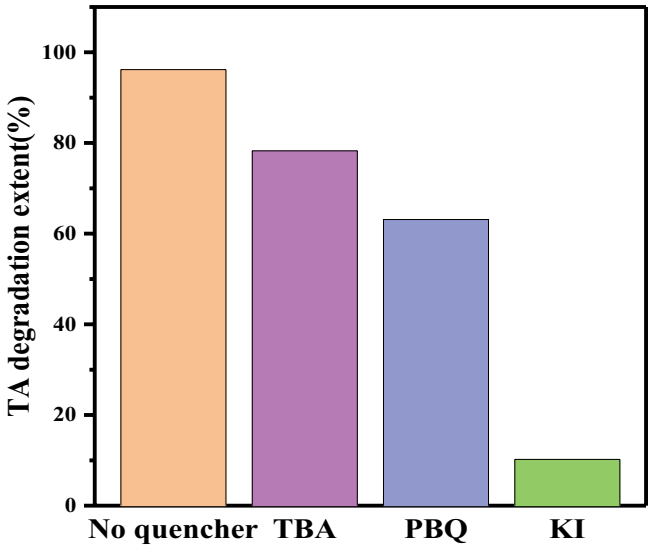

Fig. 11. Free radical capture experiment.

continued to increase, the photocatalytic activity of the prepared $Bi_{12}TiO_{20}$ powder started to decrease, and only 44.94% was obtained at 700°C. Therefore, the $Bi_{12}TiO_{20}$ material prepared by roasting at 600°C for 3 h had the best reactivity. Comparing Fig. 2b, it can be found that the peak intensity of the XRD spectra of $Bi_{12}TiO_{20}$ becomes larger when the roasting temperature increases from 450°C and only the diffraction peak of $Bi_{12}TiO_{20}$ appears, and the photocatalytic activity of $Bi_{12}TiO_{20}$ is the highest at 600°C. This shows that the well-crystallised $Bi_{12}TiO_{20}$ material has a high catalytic activity.

To study the stability of $Bi_{12}TiO_{20}$ (Bi/Ti = 12:1), it was washed, filtered and dried before use. Photocatalytic degradation experiments were carried out under the same reaction conditions (0.1 g of catalyst dosing and 5 mg/L of TA solution). Fig. 10 shows the excellent stability of this ratio of $Bi_{12}TiO_{20}$. The degradation rate of TA was still 92.99% after three repetitions, indicating that $Bi_{12}TiO_{20}$ was not deactivated and not easily photolyzed. The degradation rate of 87.60% after the fourth reuse was mainly due to the loss caused by the washing, filtering and drying steps during the reuse process, as well as some of the dye molecules causing adsorption on the $Bi_{12}TiO_{20}$ surface, resulting in the inability to desorb.

3.5. Photocatalytic mechanism

The mechanism of photocatalytic degradation of TA by $Bi_{12}TiO_{20}$ (Bi/Ti = 12:1) was investigated by the photocatalytic reaction of different radical trapping agents. The hydroxyl radical ($^{\bullet}OH$), superoxide radical ($^{\bullet}O_2^-$) and hole (h^+) were trapped by tert-butyl alcohol (TBA), p-benzoquinone (PBQ), and potassium iodide (KI), respectively [29,30]. Fig. 11 shows that the degradation of TA by this material reached 96.18% without the addition of trapping agents (i.e., blank experiment); the addition of TBA, PBQ and KI reduced the

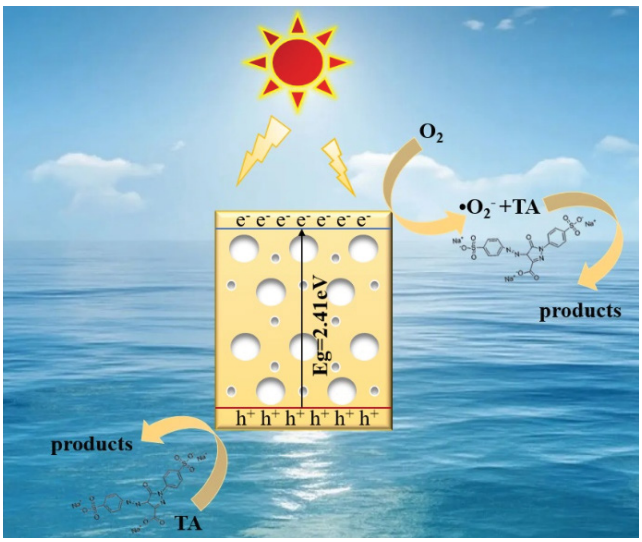

Fig. 12. Mechanism of photocatalytic degradation of tartar yellow by $Bi_{12}TiO_{20}$ (Bi/Ti = 12:1) under visible light irradiation.

degradation of TA to 78.26%, 72.12% and 10.19%, respectively. The results indicated that the active substances that played an important role in TA degradation were h^+ and $^{\bullet}O_2^-$.

Based on the results of the above radical capture experiments, the mechanism of photocatalytic degradation of TA by $Bi_{12}TiO_{20}$ (Bi:Ti = 12:1) prepared by citric acid-pyrolysis was proposed. As shown in Fig. 12, under the irradiation of visible light, the conduction band (CB) of $Bi_{12}TiO_{20}$ (Bi:Ti = 12:1) is excited to produce photoelectrons (e^-) and holes (h^+) in the valence band (VB). h^+ is a powerful oxide species that can directly participate in the degradation process of TA, decomposing it into small molecule products [31]. In turn, e^- reacts with dissolved oxygen in solution to form $^{\bullet}O_2^-$ and finally, the degradation of TA by $Bi_{12}TiO_{20}$ (Bi/Ti = 12:1) materials is enhanced by the synergistic effect of $^{\bullet}O_2^-$ and h^+.

4. Conclusion

Three types of bismuth titanate with better performance, $Bi_{12}TiO_{20}$, $Bi_4Ti_3O_{12}$ and $Bi_2Ti_2O_7$, were successfully prepared by the citric acid-pyrolysis method at a ratio of 1:1 of metal ions to citric acid substance and a roasting temperature of 600°C.

The citric acid-pyrolysis method synthesized $Bi_{12}TiO_{20}$ (Bi/Ti = 12:1) has higher crystalline properties, a loose and porous mesh structure with a forbidden band width of 2.41 eV, which is more favourable for the absorption of visible light.

The degradation of the dye TA by $Bi_{12}TiO_{20}$ (Bi/Ti = 12:1) was basically in accordance with the pseudo-first-order kinetic equations, and the degradation rate of the dye TA reached 96.18% after 150 min. The analysis of the photocatalytic mechanism showed that $^{\bullet}O_2^-$ and h^+ played a major synergistic role in the photocatalytic degradation. The strong oxidation of h^+ directly degraded TA to small molecule products, while e^- would react with dissolved oxygen in the solution to form $^{\bullet}O_2^-$, which degraded TA to small molecule products. Experiments on the recycling of $Bi_{12}TiO_{20}$ (Bi/Ti = 12:1) have shown its stable performance and the feasibility of this method for the synthesis of $Bi_{12}TiO_{20}$ in dye wastewater treatment.

Acknowledgments

This work was supported by the National Natural Science Foundation of China (grant no. 51464007, 51864010), and Guizhou Science and Technology Department (grant no. [2021]482).

References

[1] S.J. Yuan, R.M. Zhang, Research progress in dye wastewater treatment technology, Dyes Dyeing, 59 (2022) 55–62.
[2] L. Liu, Characterization of Modified Rice Straw Adsorbent and Adsorption Performance of Methylene Blue Solution, Chongqing University, China, 2011.
[3] M.C. Collivignarelli, A. Abbà, M.C. Miino, S. Damiani, Treatments for color removal from wastewater: state of the art, J. Environ. Manage., 236 (2019) 727–745.
[4] F. Salimi, M. Eskandari, C. Karami, Investigation of methylene blue adsorption in wastewater using nano-zeolite modified with copper, Desal. Water Treat., 85 (2017) 206–214.
[5] H. Abbasi, F. Salimi, F. Golmohammadi, Removal of cadmium from aqueous solution by nanocomposites of bentonite/TiO_2 and bentonite/ZnO using photocatalysis adsorption process, Silicon, 12 (2020) 2721–2731.
[6] F. Salimi, M. Abdollahifar, A.R. Karami, The effect of NaOH and KOH on the characterization of mesoporous AlOOH in the solvothermal route, Ceram. Silik., 60 (2016) 273–277.
[7] F. Salimi, M. Abdollahifar, P. Jafari, M. Hidaryan, A new approach to synthesis and growth of nanocrystalline AlOOH with high pore volume, J. Serb. Chem. Soc., 82 (2017) 203–213.
[8] A.R. Jahangiri, M. Sedighi, F. Salimi, Synthesis of zinc-sulfate nano particles and detection of their induction time, nucleation rate and interfacial tension, Iran. J. Chem. Chem. Eng., 38 (2019) 45–52.
[9] A. Benhouria, M.A. Islam, H. Zaghouane-Boudiaf, M. Boutahala, B.H. Hameed, Calcium alginate–bentonite–activated carbon composite beads as highly effective adsorbent for methylene blue, Chem. Eng. J., 270 (2015) 621–630.
[10] G. Xiong, B.B. Wang, L.X. You, B.Y. Ren, Y.K. He, F. Ding, I. Dragutan, V. Dragutan, Y.G. Sun, Hypervalent silicon-based, anionic porous organic polymers with solid microsphere or hollow nanotube morphologies and exceptional capacity for selective adsorption of cationic dyes, J. Mater. Chem. A, 7 (2019) 393–404.
[11] N.D.C.L. Beluci, G.A.P. Mateus, C.S. Miyashiro, N.C. Homem, R.G. Gomes, M.R. Fagundes-Klen, R. Bergamasco, A.M.S. Vieira, Hybrid treatment of coagulation/flocculation process followed by ultrafiltration in TiO_2-modified membranes to improve, Sci. Total Environ., 664 (2019) 222–229.
[12] R. Liu, D. Lin, C.L. Si, Mussel-inspired cellulose-based nanocomposite fibers for adsorption and photocatalytic degradation, ACS Sustainable Chem. Eng., 6 (2018) 15756–15763.
[13] S.H. Liu, S. Wang, C.S. Lei, R.Y. Li, S.Y. Feng, Q.Y. Jin, Study of the efficiency of g-C_3N_4-loaded P25 for photocatalytic degradation of malachite green in aqueous and pickering emulsion, J. Mater. Sci.: Mater. Electron., 33 (2022) 5846–5858.
[14] D. Laishram, K.P. Shejale, R. Gupta, R.K. Sharma, Heterostructured HfO_2/TiO_2 spherical nanoparticles for visible photocatalytic water remediation, Mater. Lett., 231 (2018) 225–228.
[15] Z.G. Zhu, P. Wu, G.J. Liu, X.F. He, B.Y, Qi, G.F. Zeng, W. Wang, Y.H. Sun, F.Y. Cui, Ultrahigh adsorption capacity of anionic dyes with sharp selectivity through the cationic charged hybrid nanofibrous membranes, Chem. Eng. J., 313 (2017) 957–966.
[16] C.Y. Li, T. Lou, X. Yan, Y.Z. Long, G.P. Cui, X.J. Wang, Fabrication of pure chitosan nanofibrous membranes as

effective absorbent for dye removal, Int. J. Biol. Macromol., 106 (2018) 768–774.
[17] H.C. Hao, L. Zhang, W.Z. Wang, S.M. Qiao, X.C. Liu, Photocatalytic hydrogen evolution coupled with efficient selective benzaldehyde production from benzyl alcohol aqueous solution over ZnS-Ni_xS_y composites, ACS Sustainable Chem. Eng., 7 (2019) 10501–10508.
[18] J.H. Zou, Z.T. Wang, W. Guo, B.B. Guo, Y. Yu, L. Wu, Photocatalytic selective oxidation of benzyl alcohol over ZnTi-LDH: the effect of surface OH groups, Appl. Catal., B, 260 (2020) 118185, doi: 10.1016/j.apcatb.2019.118185.
[19] K.Q. Jing, W. Ma, Y.H. Ren, J.H. Xiong, B.B. Guo, Y.J. Song, S.J. Liang, L. Wu, Hierarchical Bi_2MoO_6 spheres in situ assembled by monolayer nanosheets toward photocatalytic selective oxidation of benzyl alcohol, Appl. Catal., B, 243 (2019) 10–18.
[20] T. Shi, Y.Y. Duan, K.L. Lv, Z. Hu, Q. Li, M. Li, X.F. Li, Photocatalytic oxidation of acetone over high thermally stable TiO_2 nanosheets with exposed (001) facets, Front. Chem., 6 (2018), doi: 10.3389/fchem.2018.00175.
[21] M.Y. Li, H.P. Li, H. Zhao, T.F. Cai, Research progress of bismuth titanate in photocatalysis, Petrochemicals, 51 (2022) 459–466.
[22] M.X. He, J.M. Dong, D. Lin, X. Chen, E.G. Wang, Preparation and catalytic properties of bismuth titanate, J. Zhanjiang Normal Coll., 30 (2009) 53–56.
[23] J.F. Chen, Y. Yang, S.H. Zhao, F.K. Bi, L. Song, N. Liu, J.C. Xu, Y.X. Wang, X.D. Zhang, Stable black phosphorus encapsulation in porous mesh-like UiO-66 promoted charge transfer for photocatalytic oxidation of toluene and *o*-dichlorobenzene: performance, degradation pathway, and mechanism, ACS Catal., 12 (2022) 8069–8081.
[24] W. Guo, Y.X. Yang, Y.N. Guo, Y.Q. Jia, H.B. Liu, Y.H. Guo, Self-assembled hierarchical $Bi_{12}TiO_{20}$–graphene nanoarchitectures with excellent simulated sunlight photocatalytic activity, Phys. Chem. Chem. Phys., 16 (2014) 2705–2714.
[25] H.S. Zuo, J. Sun, K.J. Deng, R. Su, F.Y. Wei, D.Y. Wang, Preparation and characterization of Bi^{3+}-TiO_2 and its photocatalytic activity, Chem. Eng. Technol., 30 (2007) 577–582.
[26] Y.J. Ou, J.Q. Shi, Q.Q. Yan, C.L. Li, Y. Zheng, Ethanol-assisted molten salt synthesis of $Bi_4Ti_3O_{12}$/$Bi_2Ti_2O_7$ with enhanced visible light photocatalytic performance, Inorg. Chem. Commun., 133 (2021) 108867, doi: 10.1016/j.inoche.2021.108867.
[27] S.P. Patil, B. Bethi, G.H. Sonawane, V.S. Shrivastava, S. Sonawane, Efficient adsorption and photocatalytic degradation of Rhodamine B dye over Bi_2O_3-bentonite nanocomposites: a kinetic study, J. Ind. Eng. Chem., 34 (2016) 356–363.
[28] A.Q. Zhou, X.H. Xu, W.F. Yao, F.L. Zeng, B.Q. Song, Preparation of $Bi_{12}TiO_{20}$ nanopowders and their light absorption properties, J. Chem. Phys., 17 (2004) 305–308.
[29] H.C. Xiang, B.Y. Tuo, X. Song, Photocatalytic degradation of methyl orange by $Bi_{20}TiO_{32}$-montmorillonite composite, Micro Nano Lett., 8 (2020) 561–565.
[30] H.C. Xiang, B.Y. Tuo, J.W. Tian, K.M. Hu, J.L. Wang, J.G. Cheng, Preparation and photocatalytic properties of Bi-doped TiO_2/montmorillonite composite, Opt. Mater., 117 (2021) 111137, doi: 10.1016/j.optmat.2021.111137.
[31] J. Luo, W.G. Li, J.R. Ye, Y.T. Zhao, G.Y. He, H.Q. Chen, Preparation and characterization of $Bi_{12}TiO_{20}$/RGO as high-efficiency photocatalysts for degradation of dye wastewater, Diamond Relat. Mater., 123 (2022) 108890, doi: 10.1016/j.diamond.2022.108890.